

## METHOD TO IMPROVE THE QUALITY OF MOIRÉ SIGNALS BY $\pm$ FIRST-ORDER MOIRÉ FRINGES

Xinmin Wu,<sup>1</sup> Jinbang Chen,<sup>1</sup> Zhishan Gao,<sup>1</sup> Yingshi Zhu,<sup>2</sup> and Feiming Chen<sup>3</sup>

<sup>1</sup>School of Electro-Optics  
Nanjing University of Science and Technology  
Nanjing 21009, P.R. China

<sup>2</sup>Changchun Institute of Optics and Fine Mechanics  
Chinese Academy of Science

Changchun, 130022, P.R. China

<sup>3</sup>Luoyang Institute of Technology  
Luoyang, 471039, P.R. China

Received 30 April 2001

**ABSTRACT:** In an amplitude grating system of small grid pitch, the diffractive effect is distinctive. Its energy will be about 10–40% of the total energy. The diffractive light is the root cause of deterioration of the contrast and sinusoidal property of the Moiré signal. The relations between the phase of  $\pm$  first-order Moiré fringes and other factors, such as the gap of the grating pair, are analyzed. It is proposed to use  $\pm$  first-order Moiré fringes to obtain high-quality signals. © 2001 John Wiley & Sons, Inc. *Microwave Opt Technol Lett* 31: 91–93, 2001.

**Key words:** Moiré fringe; grating pair; phase

### 1. INTRODUCTION

Most Moiré fringe measurement systems of small grid pitch use a normal incident system with short-focal photoelectric receiving or direct receiving. This kind of system is simple, but the sinusoidal property of the Moiré fringe signal is not good. In particular, the poor contrast of the fringe makes the signal unstable. All of these factors affect the reliability of the measuring system. At present, most of the measuring systems are amplitude grating Moiré fringe systems, so it is necessary to improve the quality of the signal.

In an amplitude grating system of small grid pitch, the diffractive effect is distinctive. Its energy will be about 10–40% of the total energy. The diffractive light is the root cause of deterioration of the contrast of the Moiré signal and sinusoidal property.

How to eliminate the useless diffractive orders and employ the useful diffractive orders to improve the quality of Moiré fringe signals are important aspects of the research on Moiré fringe [1–3]. The authors have studied the characteristics of +first- and –first-order Moiré fringes, and propose that we can use  $\pm$  first-order Moiré fringes effectively to improve the quality of the Moiré signal.

### 2. THEORY

**2.1. Moiré Optical Field of Grating Pair.** In a general amplitude grating Moiré fringe system, the Moiré pattern of incoherent light is a kind of beat phenomenon of the modulated optical field of the grating pair. It can be explained to be the component whose frequency is smaller than that of the

original beat of the system (i.e., the spatial frequency of the grating). In a grating system, diffraction plays the main role, and the Moiré fringe is the interference fringe of the diffractive light. It can be expressed by the equation [4]

$$I = B_0 + \sum_{m=-\infty}^{\infty} B_m \exp \left[ C_m - 2\pi m \left( \frac{x_1}{\omega_1} - \frac{x_2}{\omega_2} \right) \right] \quad (1)$$

where  $B_0$  is the background intensity of the Moiré optical field,  $B_m$  is the amplitude of the  $m$ th diffractive fringe, and  $\omega_1, \omega_2$  are the grating constants of the grating pair.

**2.2. Phase Relation of +First- and –First-Order Moiré Fringes of Diffractive Grating Pair.** Figure 1 is a grating pair which is composed of two gratings with the same grating constant  $\omega$  and gap  $t$ .  $AB$  is a bundle of light. We assume an arbitrary point  $O$  in grating  $G_1$  as a zero-phase point, and establish a coordinate system with  $O$  as the origin. Its  $x$ -axis is perpendicular to the rulings of  $G_1$ , and the  $y$ -axis is parallel to the rulings of  $G_1 \cdot CN \perp G_1$ . The coordinate of  $N$  is  $(x, y)$ .

In this system, it is easy to prove that, if the sum of  $p_i$  and  $q_i$  of their order sequence  $(p_i, q_i)$  is equal ( $i$  and  $j$  are integers), for example,  $p_1 + q_1 = p_2 + q_2 = r$ , both of the diffractive light will exit in the same direction. This direction is the same as that of the  $p + q = r$ th-order diffractive light from a single grating. This group of light is defined as the  $r$  group. Only for the direction of incident light and emergent light is the effect of the grating pair with two identical pitch and parallel rulings equivalent to that of a single grating with the same pitch. The  $r$  group can be represented by  $(p, r - p)$ , where  $r = p + q$ .

In Figure 1, the phase will change  $\delta_B$  after the incident light  $AB$  passes through  $G_1$ . The  $p$ th-order diffractive light of  $G_1$  passes through the gap of  $t$ , and the phase change is  $(2\pi/\lambda)(t/\cos \beta)$ . Then it passes through  $G_2$ , and the phase of the  $(r - p)$ th-order diffractive light will change  $\delta_C$ . So the phase of the emergent light of order sequence  $(p, r - p)$  at  $C$  can be written as follows:

$$\Phi_C = \Phi_B + \delta_B + \frac{2\pi}{\lambda} \frac{t}{\cos \beta} + \delta_C \quad (2)$$

where  $\Phi_B$  is the phase of incident light at  $B$  before it passes through  $G_1$ .

The phase at point  $C$  of light passing through  $G_1$  and  $G_2$  can be expressed by the fractional position and fractional displacement [5, 6] as follows:

$$\Phi_C = K_p + \frac{2\pi}{\lambda} (x \sin \alpha'' + y \sin \alpha') + \frac{2\pi}{\lambda} \frac{t}{\cos \beta} + 2\pi r f + 2\pi p \rho \quad (3)$$

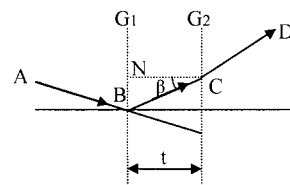


Figure 1 Light ray of diagram of grating pair

where  $f$  and  $\rho$  are the fractional position and fractional displacement of point  $C$ , respectively.  $K_p$  is a phase function related to the structure of the grating pair. It is a constant for a definite grating pair.  $\alpha''$ ,  $\alpha'$  are the angles between  $AB$  and the principal median plane, and  $AB$  and the secondary median plane, respectively. When the rulings of the two gratings are parallel, they equal zero.

Since, in amplitude grating diffractive systems, most energy concentrates on 0,  $\pm$ first-order diffractive light, we focus on the research of  $(0, +1)$ ,  $(+1, 0)$ ,  $(0, -1)$ , and  $(-1, 0)$ -order light beams. The interference fringes of  $(-1, 0)$  and  $(0, -1)$  diffractive light are called  $-$ first-order Moiré fringes. The interference fringes of  $(+1, 0)$  and  $(0, +1)$  diffractive light are called  $+$ first-order Moiré fringes.

The diagram of  $+$ first-order and  $-$ first-order Moiré fringes is shown in Figure 2.  $G_1$  and  $G_2$  have the same grid pitch. Their rulings are parallel. There is a small angle  $\theta_j$  between their normal lines.  $L$  is the imaging lens.  $(0, -1)$  and  $(-1, 0)$ -order Moiré fringes focus on  $F_{-1}$ ;  $(0, +1)$  and  $(+1, 0)$ -order Moiré fringes focus on  $F_{+1}$ .

Since the phases of  $(0, +1)$  and  $(0, -1)$ -order fringes at  $G_2$  are equal, the phase relation of signals at  $F_{-1}$  and  $F_{+1}$  depends on the phase relation of  $(-1, 0)$  and  $(+1, 0)$ -order light beams at the exit plane. From Eq. (3), Figure 2, and the grating equation, the phase difference of Moiré fringes at  $F_{-1}$  and  $F_{+1}$  is expressed by the equation

$$\Delta\Phi = \frac{2\pi t}{\lambda} [\cos(\theta_j - \theta_{-1}) - \cos(\theta_j + \theta_{+1})] + 2m\pi + \Delta'$$

$$- \frac{2\pi t \cos \theta_j}{\omega} \left[ \frac{\sin \theta_{-1}}{\cos(\theta_{-1} - \theta_{+1})} + \frac{\sin \theta_{+1}}{\cos(\theta_j - \theta_{+1})} \right]$$

$$- \frac{2\pi t}{\lambda} \cos \theta_j \sin \theta_i \left[ \frac{\sin \theta_{+1}}{\cos(\theta_j - \theta_{+1})} + \frac{\sin \theta_{-1}}{\cos(\theta_j - \theta_{+1})} \right] \quad (4)$$

where  $m$  is an integer, and  $\Delta'$  is the phase difference caused by  $F_{-1}$  and  $F_{+1}$  not being in the same plane. When  $\theta_i$  and  $\theta_j$  are fixed,  $\Delta'$  does not change.

From Eq. (4), it can be seen that the phase difference  $\Delta\Phi$  is decided by a gap of the grating pair, the incident angle  $\theta_i$  on the grating pair, and the parallelism  $\theta_j$  of  $G_1$  and  $G_2$ . For a given grating pair, we can make the phase of the Moiré fringe at  $F_{-1}$  and  $F_{+1}$  opposite by adjusting these parameters. Then the signals are received by the two phototriodes placed at  $F_{-1}$  and  $F_{+1}$ , and are put into a differential amplifier. A high-quality Moiré fringe signal with high contrast and low noise can be obtained.

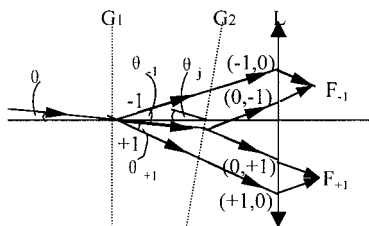


Figure 2 Diagram of  $+$ first- and  $-$ first-order Moiré fringes

### 3. EXPERIMENTS

The dynamic motion of the Moiré fringe of long grating must have a stable and uniform velocity. In order to achieve repeated measurement, the index grating should move a long distance. This will make the experimental setup complicated. So we use a radial grating pair on a circle dividing the equipment to measure the relations of the phase difference versus the factors in Eq. (4).

The schematic diagram of the experimental setup is shown in Figure 3. The gratings used here are two concentric small grid pitch radial gratings. Their total rulings are 324,000 lines, and the grid pitch is 0.02 mm. The light source is a 6 V 5 W voltage-stabilized instrumental bulb. In order to improve the contrast of the Moiré fringe and reduce the influence of divergence of the light source, the system needs a parallel beam vertically projected on the grating pair. So the filament must be placed in the focus of collimator lens  $L_1$  and parallel to the rulings of the gratings. By calculation [4], we use a spiral filament whose diameter is 1 mm and length is 5 mm. Thus, the emergent light is a plane wave. The diameter of the phototriode is 2.5 mm, and its peak wavelength is 0.85  $\mu\text{m}$ . The scaled grating revolves around its axis  $oo'$  uniformly. The diameter of  $L_2$  must be large enough to receive all of the light emerging from the grating pair. Its focal length must be long enough that the 0,  $\pm$ first-order Moiré fringes are separated to place the phototriodes. According to the principle of geometrical optics, the calculated parameters of  $L_1$  are diameter  $> 30$  mm, focal length  $> 60$  mm. The lens we used here has diameter = 60 mm and focal length = 100 mm.

Light from the bulb collimated by  $L_1$  projects on the grating pair. The Moiré fringes focus on the phototriodes which are in the focal plane of  $L_2$ . The  $+$ first- and  $-$ first-order Moiré fringes are symmetrically located at the two sides of the zero-order fringe. The phototriodes are placed at  $F_{-1}$  and  $F_{+1}$  to receive the  $+$ first- and  $-$ first-order Moiré fringes. Then the signals are treated, and their phase difference can be read accurately. The relation curves of the phase difference  $\Delta\Phi$  versus  $\Delta t$  are shown in Figure 4 under two circumstances.

### 4. CONCLUSION

It can be seen that the measured results agree with the theoretical analysis. The parallelism of the two gratings, the incidental angle on the grating pair, and the change of the gap of the two gratings, are the main causes of the phase difference. When  $\theta_i = \text{constant}$ , the change of  $\theta_j$  produces a small influence on  $\Delta\Phi$ , as shown in Figure 4(a). When  $\theta_j = \text{constant}$ , the change of  $\theta_i$  produces a great influence on  $\Delta\Phi$  as shown in Figure 4(b). The relation of  $\Delta\Phi$  versus  $\Delta t$  is linear. We can obtain two antiphase Moiré fringes by adjust-

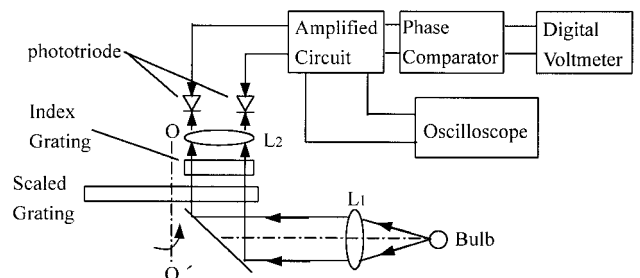
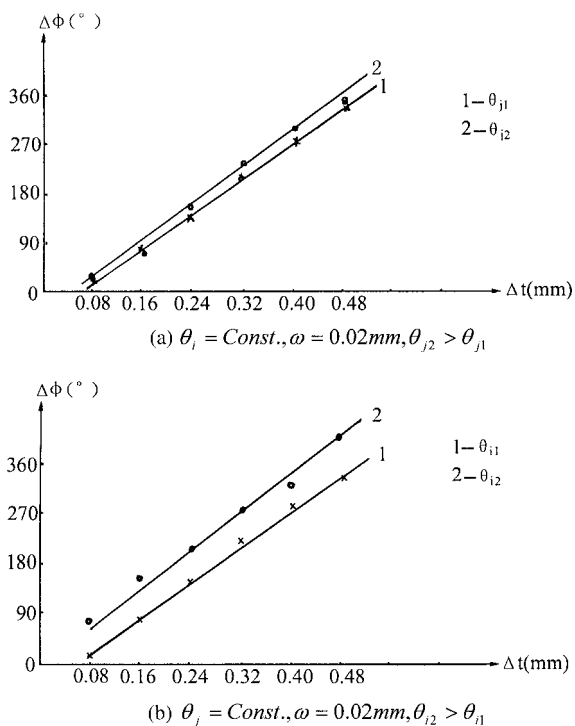


Figure 3 Block diagram of experimental setup



**Figure 4** Experimental results of  $\Delta\Phi$  versus  $\Delta t$  under different circumstances

ing the gap of the grating pair  $t$ . Then, under the condition of a given grating pair, we can obtain a high-contrast and good sinusoidal Moiré signal. This is useful in practical grating measurement systems.

## REFERENCES

1. B.J. Kim and J.S. Song, Determination of small angular displacement by Moiré fringes of matched radial-parallel gratings, *Appl Opt* 36 (1997), 2848–2855.
2. M. De Angelis, S. De Nicola, P. Ferraro, A. Finizio, and G. Pierattini, Analysis of Moiré fringes for measuring the focal length of lenses, *Opt Lasers Eng* 30 (1998), 279–286.
3. M. Ohler and J. Haertwig, Theory of Moiré fringes for X-ray diffraction topographs of bicrystals, 55 (1999), 413–422.
4. O. Kafri and I. Glatt, *The physics of Moiré metrology*, Wiley, New York, 1990.
5. Z. Shanzhong and H. Weishi, *Technology of metrology gratings*, Mechanical Industry Publishing House of China, Beijing, P.R. China, 1985.
6. J. Guild, *The interference system of crossed diffraction grating*, Clarendon, Oxford, England, 1956.

© 2001 John Wiley & Sons, Inc.

## RESEARCH ON DYNAMICS IN MODULATION-DOPED GaAs/Al<sub>x</sub>Ga<sub>1-x</sub>As HETEROSTRUCTURES

Guo-Hui Li,<sup>1</sup> Shi-Ping Zhou,<sup>2</sup> and De-Ming Xu<sup>1</sup>

<sup>1</sup>Department of Communication Engineering  
Shanghai University  
Shanghai 200072, P.R. China

<sup>2</sup>Department of Physics  
Shanghai University  
Shanghai 201800, P.R. China

Contract grant sponsor: National Natural Science Foundation of China.

Contract grant numbers: 69871016.

**ABSTRACT:** We discuss the dynamics of the forced modulation-doped Al<sub>x</sub>Ga<sub>1-x</sub>As heterostructure device governed by the coupled differential equations, which is operative in the state far from thermodynamic equilibrium. Biased with an appropriate dc field, the system exhibits two states: spontaneous current oscillation and fixed points. Under an ac driving force imposed on a dc bias, the dynamical system shows the expected characteristics of frequency locking, quasiperiodicity, and chaos, which are sensitive to the amplitude and frequency of the external applied microwave field. In particular, the basins of attraction of both an ordinary attractor and a chaotic attractor are presented. © 2001 John Wiley & Sons, Inc. *Microwave Opt Technol Lett* 31: 93–95, 2001.

**Key words:** chaos; heterostructure; negative differential conductivity

## 1. INTRODUCTION

Negative differential conductivity (NDC) and electrical current instabilities in modulation-doped semiconductor heterostructures have been extensively investigated in the last three decades [1–2]. A basic physical mechanism about the self-sustained oscillation has been presented in [2]. For a GaAs heterostructure, the real space transfer of hot electrons from high-mobility undoped GaAs to low-mobility heavily  $n$ -doped Al<sub>x</sub>Ga<sub>1-x</sub>As layers occurs, leading to an N-shaped current–voltage characteristic. It is also found that the interaction between the self-sustained oscillation and an external periodical force can result in various interesting phenomena, such as frequency locking, quasiperiodicity, and chaos [3–8].

Layered semiconductor heterostructures are chosen to be studied because of their current importance, both in basic research and in microelectronics applications. Since Aoki, Kobayashi, and Yamamoto [4] first observed the chaotic behavior in  $n$ -type GaAs semiconductors in 1982, the nonlinear chaotic dynamics in semiconductors have become of considerable interest both in experiment [5, 6] and in theory [6, 7]. Because modern electronic devices may encounter serious chaotic noise which prevents normal operation, it is important to understand how a nonlinear device responds to the external fields.

In this paper, we mainly focus on the numerical simulations of the dynamical equations to investigate the dynamical behavior of Al<sub>x</sub>Ga<sub>1-x</sub>As heterostructures depending on the frequency and amplitude of the external applied microwave field. Numerical simulation indicates that both a periodically oscillation attractor and a fixed-point attractor can coexist under an appropriate dc bias. The basins of attraction of period 3 and chaotic attractors are also computer simulated.

## 2. STATIC CHARACTERISTICS

In our simple model, the nonlinear electron transport processes are described by the differential equations which have been derived in [9]. To simplify matters, equations are expressed in a dimensionless form by defining dimensionless quantities as  $X = n_1/N_D$ ,  $Y = \mu_1 E_{\parallel}/V_{ds}$ ,  $Z = \phi_B/K_B T_L$ , and  $T = t/\tau_E$ .

The static current density–field characteristic is shown in Figure 1. The fixed points of the dynamical system are denoted by \*. The real space transfer of electrons leads to NDC as the bias voltage value  $U_0$  exceeds 36.7 V, where the dynamical system shows spontaneous current (voltage) oscillation at frequencies of 100 GHz. The load line (the straight line) is shifted in parallel with the varying applied bias voltage. Consequently, a suitable dc bias that lies within the